Rev. Roum. Sci. Techn.– Électrotechn. et Énerg.
Vol. **67**, *3*, pp. 265–270, Bucarest, 2022

INCIPIENT SHORT CIRCUIT FAULT IMPACT ON SERVICE CONTINUITY OF AN ELECTRIC VEHICLE PROPELLED BY DUAL INDUCTION MOTORS STRUCTURE

SALAH YAHIA CHERIF[1], DJAMEL BENOUDJIT[1,2], MOHAMED SAID NAIT-SAID[1], NASREDDINE NAIT-SAID[1]

Keywords: Induction motor; Backstepping control; Turn-to-turn fault; Electric vehicle; Propulsion Structure.

The short circuit is among one of the most dangerous electrical faults in induction motors, which leads to serious implications on the motor operation and its performance. The present paper deals with the influence of the stator short circuit fault in its early stage in terms of performance and service continuity of an electric vehicle (EV) using a dual induction motor's structure piloted by Backstepping control. An equivalent induction motor model with turn-to-turn fault on one stator phase, without already assuming the temperature effect through an intrinsic model, is investigated. Afterward, its impacts on electric vehicle performance using simulation tests are presented and discussed.

1. **INTRODUCTION**

A motor control system with high robustness is an important issue in research [1]. Thus, it is evident that the monitoring and diagnosis of electrical machines constitute an economic and scientific challenge, combining safety and continuity of service for electrical drives. The faults in an induction motor are generally classified as either electrical or mechanical faults [2]. About 35 % to 40 % of the total failures of induction motors take place due to electrical faults [2–5]. The stator winding insulation failure due to a short-circuit known as an inter-turn short-circuit is one of the most common and severe electrical faults affecting the electric motor [6–8]. This is mainly due to long-term thermal aging and, ultimately, insulation failure [2]. If the stator turns are shorted, a sizeable circulating current is induced in shorted turn, so the thermal overloading [9]. However, during operational phases, electric motors are continuously exposed to thermal, mechanical, and vibrational effects. Therefore, it is important to detect and identify any incipient fault that occurs within the electrical motor at its earliest stage to avoid any unplanned outage, particularly in applications where safety is the primary concern of the global system. On the side, it is common for any vehicle in urban traffic to require regime changes, frequent acceleration, deceleration, cruising, and stopping phases, which lead to serious breakdowns. In those applications where downtime isn't acceptable, and continuity of service is required, an unpredicted failure of a motor might result in higher maintenance costs or loss of life. However, understanding fault diagnosis is very important because a good diagnosis is early detection of the severity and location of faults to reduce the downtime and maintenance costs while ensuring continuity of operations for an EV. Therefore, modeling and identifying inter-turn short circuit faults at the earliest stage of an induction motor is the first significant step in the motor health monitoring and fault diagnosis process.

To minimize performance degradation and avoid dangerous situations, numerous research studies in the literature regarding stator winding inter-turn short circuit modeling and analysis have been proposed [10–17].

The present work describes a simulation study of stator winding short-circuit fault effects, *which* occurred at its earliest stage in the first phase into one of both motors of an electric vehicle propelled by a dual induction motors structure under several short-circuited levels, in terms of vehicle performances and service continuity during steering maneuvers, based on an accuracy faulty model.

The proposed control structure consists of an electric vehicle using dual-induction motors and backstepping control placed at the rear wheels, which propels electrically the vehicle, based on an electric differential assured by dual motors operating at a different speed. For this purpose, a precise equivalent model of an induction motor (IM) considering the turn-to-turn fault resulting from a short-circuit winding in the first stator phase at several levels is described. The consequences on an electric vehicle in terms of performance and service continuity where a fault occurred in one of both propulsion structure motors are analyzed.

Simulation tests were carried out to detect fault occurrence and its impact on EV control without already considering the temperature effect through an intrinsic model for a faulty model. Also, note that the existence of the short-circuit in some turns on one phase could give an increase in temperature inside the machine leading to overheating, which causes the insulation loss of the machine winding, and the short-circuit becomes rapid and total in such a small time.

The paper is organized as follows. Section 2 presents the Backstepping control for IM, using an accurate faulty model with a turn-to-turn fault applied for an EV. In section 3, the dual-motor configuration of the proposed propulsion structure will be shown. To evaluate the performances and the effect of the failure caused by a turn-to-turn fault in the first stator phase of the suitable motor, a series of simulation tests will be presented in section 4. The conclusion is done in section 5.

2. **BACKSTEPPING CONTROL FOR IM**

The backstepping control technique enables in a sequential and systematic manner to build stabilizing Lyapunov function. Thus, the main goal is to achieve the convergence of errors towards zero and stable operations of the system.

[1] LSP-IE'2000 Laboratory, Electrical Engineering department, University of Batna 2, 05000, Batna, Algeria
[2] Health and Safety Institute, University of Batna 2, 53 Constantine Street, 05078, Batna, Algeria
E-mails: s.yahiacherif@univ-batna2.dz, d.benoudjit@univ-batna2.dz, m.naitsaid@univ-batna2.dz, n.naitsaid@univ-batna2.dz

The design of backstepping control approach is to recursively select the appropriate state variables as a virtual reference input, characterized by step-by-step interlacing. Each step generates a new virtual control variable, and finally, the process terminates when the final external control is reached [18–22]. This is used to maintain stability and better performance capabilities of the system under disturbances, with at least two control loops.

Let us first give the equations of an IM for a healthy model, which includes both the mechanical and electrical dynamics, expressed in the (*d*, *q*) synchronous rotating frame obviously, after orientation of the rotor flux by [1, 19]:

$$\begin{aligned}
\frac{\mathrm{d}\Omega}{\mathrm{d}t} &= \frac{pM}{JL_r}\phi_r i_{sq} - \frac{T_L}{J} \\
\frac{\mathrm{d}\phi_r}{\mathrm{d}t} &= \frac{M}{T_r} i_{sd} - \frac{1}{T_r}\phi_r \\
\frac{\mathrm{d}i_{sd}}{\mathrm{d}t} &= -\left(\frac{R_s}{\sigma L_s} + \frac{M^2 R_r}{\sigma L_s L_r^2}\right) i_{sd} + \omega i_{sq} + \frac{MR_r}{\sigma L_s L_r}\phi_r + \frac{1}{\sigma L_s}\nu_{sd} \\
\frac{\mathrm{d}i_{sq}}{\mathrm{d}t} &= -\left(\frac{R_s}{\sigma L_s} + \frac{M^2 R_r}{\sigma L_s L_r^2}\right) i_{sq} - \omega i_{sd} - \frac{M\omega_r}{\sigma L_s L_r}\phi_r + \frac{1}{\sigma L_s}\nu_{sq}.
\end{aligned} \tag{1}$$

The objective of the Backstepping design is to synthesize the *d*-axis and *q*-axis voltage control input expressions (v_{sd}^*, v_{sq}^*), where the system must be able to follow the desired references. It mainly consists of the following two steps.

For the first step, the objective is to replace the classical PI tracking controller by computing the reference values of stator current components (i_{sd}^*, i_{sq}^*).

In our case, the tracking errors dynamics of speed ($\dot{e}_\Omega$) and rotor flux ($\dot{e}_\phi$), using eq. (1) are defined as follows:

$$\begin{cases}
\dot{e}_\Omega = \dot{\Omega}^* - \dot{\Omega} = \dot{\Omega}^* - \dfrac{1}{J}\dfrac{pM}{L_r}\phi_r i_{sq} + \dfrac{T_L}{J} \\
\dot{e}_\phi = \dot{\phi}_r^* - \dot{\phi}_r = \dot{\phi}_r^* - \dfrac{M}{T_r} i_{sd} + \dfrac{1}{T_r}\phi_r
\end{cases}. \tag{2}$$

Then, with an appropriate choice of the Lyapunov function V_1 of the subsystem described above, such that:

$$V_1 = \frac{1}{2}\left(e_\Omega^2 + e_\phi^2\right). \tag{3}$$

For which its derivative $\dot{V}_1$ must be negative, we can write:

$$\begin{cases}
\dot{e}_\Omega = -k_\Omega \cdot e_\Omega \\
\dot{e}_\phi = -k_\phi \cdot e_\phi
\end{cases}, \tag{4}$$

where k_Ω, k_ϕ are positive coefficients to guarantee stable tracking. Thereby, the reference values of stator current components are given by:

$$\begin{cases}
i_{sd}^* = \dfrac{JL_r}{pM\phi_r}\left(\dot{\Omega}^* + k_\Omega \cdot e_\Omega + \dfrac{1}{J}T_r\right) \\
i_{sq}^* = \dfrac{T_r}{M}\left(\dot{\phi}_r^* + k_\phi \cdot e_\phi + \dfrac{1}{T_r}\phi_r\right)
\end{cases}. \tag{5}$$

In the second step, the main goal is to achieve the final external control by computing the reference stator voltage. To do so, we define the stator current error terms. Expressed by their derivatives as follows:

$$\begin{cases}
\dot{e}_{id} = \dot{i}_{sd}^* - \dot{i}_{sd} \\
\dot{e}_{iq} = \dot{i}_{sq}^* - \dot{i}_{sq}
\end{cases}. \tag{6}$$

Substituting (1) into (6), we find:

$$\begin{cases}
\dot{e}_{id} = \dot{i}_{sd}^* - d_1 - \dfrac{1}{\sigma L_s}\nu_{sd} \\
\dot{e}_{iq} = \dot{i}_{sq}^* - d_2 - \dfrac{1}{\sigma L_s}\nu_{sq}
\end{cases}, \tag{7}$$

where

$$\begin{cases}
d_1 = -\left(\dfrac{R_s}{\sigma L_s} + \dfrac{M^2 R_r}{\sigma L_s L_r^2}\right) i_{sd} + \omega_s i_{sq} + \dfrac{MR_r}{\sigma L_s L_r}\phi_r \\
d_2 = -\left(\dfrac{R_s}{\sigma L_s} + \dfrac{M^2 R_r}{\sigma L_s L_r^2}\right) i_{sq} - \omega_s i_{sd} - \dfrac{MR_r}{\sigma L_s L_r}\phi_r
\end{cases}. \tag{8}$$

One can notice that system (7) includes the system inputs (the stator voltage). These could be found through the definition of a new Lyapunov function based on the errors of the speed, the rotor flux, and of the stator currents.

From the equations system (7), the stator voltage input could be calculated through the definition of another Lyapunov function in the following form:

$$V_2 = V_1 + \frac{1}{2}\left(e_{id}^2 + e_{iq}^2\right). \tag{9}$$

To ensure that its derivative is always negative, such that

$$\dot{V}_2 = \dot{V}_1 - k_{id}e_{id}^2 - k_{iq}e_{iq}^2. \tag{10}$$

with k_{id}, k_{iq} are positives coefficients.

Finally, the input voltages components are chosen as follows:

$$\begin{cases}
v_{sd}^* = \sigma L_s (\dot{i}_{sd}^* - d_1 + k_{id}e_{id}) \\
v_{sq}^* = \sigma L_s (\dot{i}_{sq}^* - d_2 + k_{iq}e_{iq})
\end{cases}. \tag{11}$$

For a faulty model, different research works of mathematical models regarding inter-turn short-circuit faults in the stator of an induction motors can be found in literature [10–17, 23–25]. As the need for greater accuracy in induction motor modeling, important physical characteristics must be considered. An accurate model for an induction motor with stator winding turn fault in first phase was presented in [25].

Stator, rotor and short-circuit equations in matrix form for an IM faulty model in αβ coordinates referred to the stator frame, with a turn-to-turn fault in the first phase "a", is formulated as follows [25], given next by eq. (12). Index *sc* denotes short circuit. Conventional used abbreviation of the induction motor will be defined next in nomenclature.

$$\nu = D_{1sc} I + \left[\omega D_{2sc} + D_{3sc}\frac{\mathrm{d}I}{\mathrm{d}t}\right], \tag{12}$$

with:

$$D_{1sc}=\begin{bmatrix} R_s & 0 & 0 & 0 & -\sqrt{\frac{2}{3}}x_{sc}R_s \\ 0 & R_s & 0 & 0 & 0 \\ 0 & 0 & R_r & 0 & 0 \\ 0 & 0 & 0 & R_r & 0 \\ \sqrt{\frac{2}{3}}x_{sc}R_s & 0 & 0 & 0 & -(R_s+x_{sc}R_s) \end{bmatrix},$$

$$D_{2sc}=\begin{bmatrix} 0 & 0 & 0 & 0 & 0 \\ 0 & 0 & 0 & 0 & 0 \\ 0 & M & 0 & L_r & 0 \\ -M & 0 & -L_r & 0 & \sqrt{\frac{2}{3}}mx_{sc} \\ 0 & 0 & 0 & 0 & 0 \end{bmatrix},$$

$$D_{3sc}=\begin{bmatrix} L_s & 0 & M & 0 & 0 \\ 0 & 0 & 0 & M & 0 \\ M & 0 & L_r & 0 & -\sqrt{\frac{3}{2}}mx_{sc} \\ 0 & M & 0 & L_r & 0 \\ x_{sc}\sqrt{\frac{2}{3}}L_s & 0 & mx_{sc}\sqrt{\frac{3}{2}} & 0 & -x_{sc}^2L_s \end{bmatrix}.$$

The voltage and current matrices are expressed as:

$$v=\begin{bmatrix} v_{s\alpha} & v_{s\beta} & 0_{r\alpha} & 0_{r\beta} & 0_{sc} \end{bmatrix}^{\mathrm{T}},\ I=\begin{bmatrix} i_{s\alpha} & i_{s\beta} & i_{r\alpha} & i_{r\beta} & i_{sc} \end{bmatrix}^{\mathrm{T}}.$$

The short-circuited turns index is:

$$x_{sc}=\frac{n_{sc}}{n}=\frac{\text{Number of interturns short - circuit windings}}{\text{Total number of interturns in healthy phase}}.$$

Figure 1 shows a general block diagram implementation of Backstepping control intended to EV application.

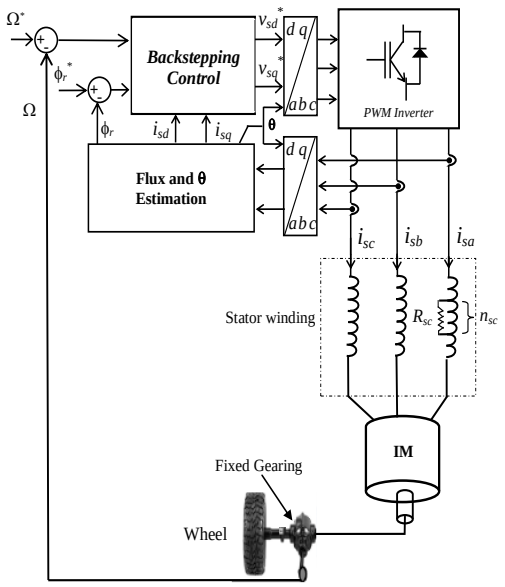

Fig. 1 – Backstepping structure of IM with turn-to-turn fault on phase *a*.

This is used to maintain stability and better performance capabilities of the system under disturbances, with at least two control loops. As shown in Fig. 1, n_{sc} represents several shortened turns in the first stator phase *a*. R_{sc} is an equivalent resistance of the shortened turns.

When the short-circuit fault is negligible (x_{sc} = R_{sc} = 0), the previous formulation gives precisely the same as in the healthy model.

3. ELECTRIC VEHICLE DUAL INDUCTION MOTOR'S STRUCTURE

Figure 2 presents the proposed control structure in which two identical induction motors drive separately the rear wheels of the vehicle via fixed gearing. The left and right induction motors are fed through power converters and driven by the backstepping strategy.

The differential action assured by dual motors operating at different speeds enables the wheels to be driven at different speeds when cornering the outer wheel covering a greater distance than the inner wheel. Then the propulsion control structure placed at the rear wheels propels electrically the vehicle and assures the required differential speed Ω_{diff} according to [26]:

$$\begin{cases} \Omega_1^*=\Omega_o^*+\Omega_{diff}^* \\ \Omega_1^*=\Omega_o^*-\Omega_{diff}^* \end{cases}, \tag{13}$$

where: Ω_1^*, Ω_2^* – speeds of left motor 1 and right motor 2, Ω_o^*, Ω_{diff}^* – EV speed command, speed difference.

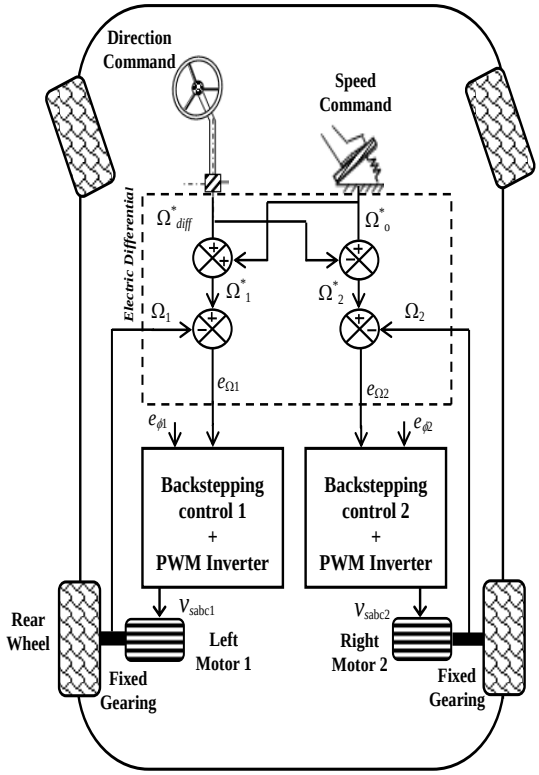

Fig. 2 – EV propulsion control structure.

4. SIMULATION RESULTS AND DISCUSSION

Numerical simulations have been conducted to assess the effect of initial turn-to-turn faults on electric vehicle structure performances propelled by dual induction motors. The data are summarized in the appendix.

Figures 3(a,b,c) and their respective zoom in Fig. 3(a_1, b_1) also Fig. 3(a_2, b_2, c_2) depict and compare the main characteristics (speed, electromagnetic torque, stator currents, and copper losses responses) of an EV propulsion

structure using dual inductions motors driven by Backstepping control where the turn-to-turn fault resulting of a short-circuit winding may occur in the first stator phase into one of both propulsion motors structure (the suitable motor) at several short-circuited turns index levels: x_{sc} = 20 %, 50 %, and 100 %.

The simulation tests were used considering the selected route defined as illustrated in Fig. 3 by the vehicle speed reference drawn in a dashed line. From scratch, the vehicle starts with constant acceleration until it attains the speed of 157 rad/s, then it will be maintained constant. In this propulsion structure, each of both motors is associated with a fixed mechanical gearing, which reduces the motor speed to the desired wheel speed and high substantial torque. At t = 0.5 s, a load torque is applied to each motor. This last case might occur, for example, when EV wheels are stopped by a strong obstacle. After there, at t = 1 s, the vehicle accomplishes its turn maneuvers by turning left. The electric differential action allows the inner wheel to rotate slower than the outer one, *i.e.*, $\Omega_{Righ} > \Omega_{left}$. Further, to test severely the propulsion structure performances, at t = 1.5 s, the turn-to-turn fault resulting from a short-circuit winding in the first stator phase has been activated on the suitable motor when the vehicle accomplishes its turn maneuvers. Finally, the vehicle maintains a constant cruising speed, which equals both motor's speeds, *i.e.*, $\Omega_{Righ} = \Omega_{left}$.

Figure 3a and its zoom in Fig. 3a$_1$ show before and after the shorted turns faulty case for x_{sc} =20%, introduced at t = 1.5 s, the simulated EV speed, electromagnetic torque, and stator currents waveforms.

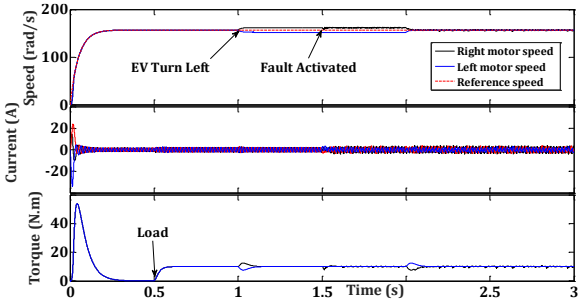

Fig. 3a – Turn-to-turn fault effect for x_{sc} = 20 %.

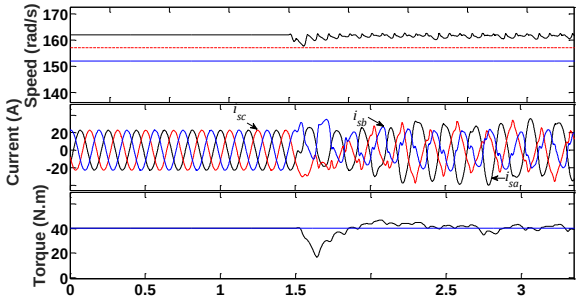

Fig. 3a$_1$ – Zoom of turn-to-turn fault effect for x_{sc} = 20 %.

The fault effect, in this case, isn't noticeable on the EV speed and electromagnetic torque responses, except for the stator currents amplitudes, which increase slightly after a fault occurs. So, in this case, the incipient winding fault will not impose a significant influence on EV performances.

Figure 3a$_2$ shows with the same above shorted turn faulty case for x_{sc} = 20 %, the evolution of stator copper losses versus time. It is well known that copper losses depend on the square of stator current in RMS value and the stator resistance. These losses resulting from Joule heating are caused by stator current induced in the stator windings, which generates the heat, and therefore the motor's temperature rises with time. Indeed, as can be seen from Fig. 3a$_2$, as the stator currents amplitudes increase, the copper losses also increase with time, particularly when the fault occurs.

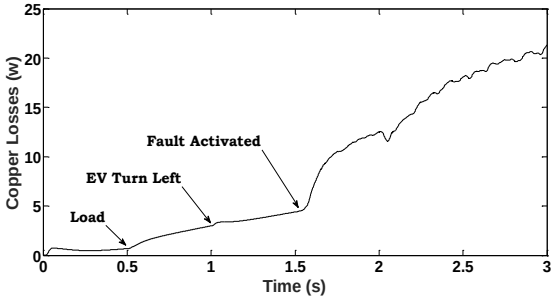

Fig. 3a$_2$ – Cooper losses evolution for x_{sc} = 20 %.

On the other hand, as shown in Fig. 3(b-c) and 3(b$_1$) the fault effect is more noticeable as the fault severity increases. For x_{sc} = 50 %, and, for x_{sc} = 100 %, while the stator current amplitude of the faulty phase current becomes higher.

The increase in RMS stator currents may have a serious damage, such as total short-circuit of the stator winding, the degradation of the insulation of the windings due to the resulting overheating, which potentially shortening its lifespan and even fire.

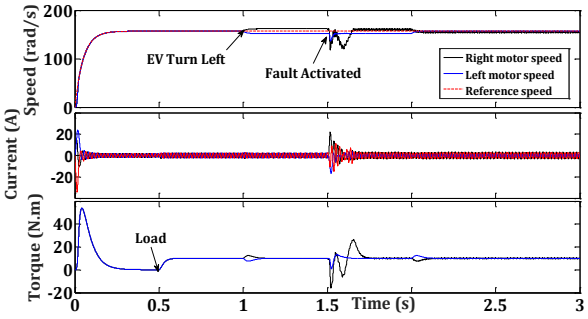

Fig. 3b – Turn-to-turn fault effect for x_{sc} = 50 %.

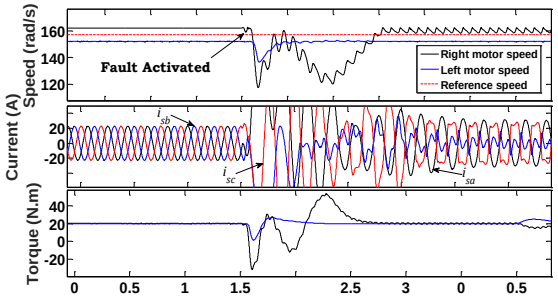

Fig. 3b$_1$ – Zoom of turn-to-turn fault effect for x_{sc} = 50 %.

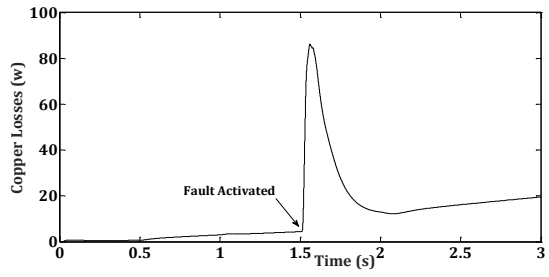

Fig. 3b$_2$ – Cooper losses evolution for x_{sc} = 50 %.

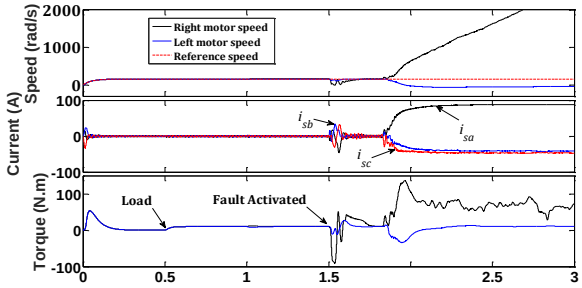

Fig. 3c – Turn-to-turn fault effect for x_{sc} = 100 %.

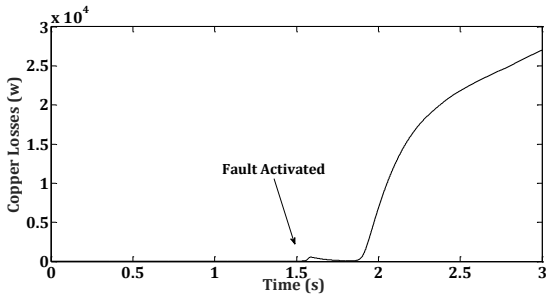

Fig. 3c$_2$ – Cooper losses evolution for x_{sc} = 100 %.

At the same time, the occurred fault cited above might influence one of the dual induction motors, which could be conducted an unbalance in the dual used motors and from which the vehicle leaves its reference trajectory, so the control of the differential action is gravely lost accompanied by the loss of the aim control vehicle direction.

Finally, as depicted in Fig. 3(b$_2$, c$_2$), with rising amplitude currents, the copper losses increase also.

The Backstepping controllers' parameters are chosen as follows:

– speed gain k_Ω = 50 000
– rotor flux gain k_ϕ = 1 000
– direct stator current gain k_{id} = 80 000
– quadrate stator current gain k_{iq} = 2 000.

They are chosen positive constants to satisfy convergence conditions and the global asymptotic stability of the system.

5. **CONCLUSIONS**

In this paper, we focused on the incipient turn-to-turn fault influence on EV dual induction motor structure performances and service continuity. An accurate model for an induction motor with an inter-turn fault in the first phase of stator winding occurred into one of both motors has been presented for detecting fault occurrence and its impact on EV control without considering the temperature effect through an intrinsic for a faulty model. Simulation tests performed under a fault severity index at several levels show that the incipient turn-to-turn short circuit fault has a negligible effect on a lower-level fault on EV operation. In this case, the vehicle continued to function even in a fault. But for the high fault levels, the results show a very significant change, particularly for the current waveforms. The stator currents amplitude raised significantly where the fault has occurred and a relative height that is lower for the other phases. Thus, if no coping measures are applied, this will result in a temperature increase in the stator winding, which will lead to the failure of the entire phase eventually. That, unfortunately, means the loss of systematic control on the EV driven by the propulsion structure.

The investigation of the impact of other stator winding faults, such as a turn-to-turn short-circuit fault in more than one phase and a phase-to-ground, based on fault-tolerant control techniques, on electric vehicle structure performances under different faults and load conditions, the use of robust observers to estimate the severity of the short circuit fault, as well as the implementation and experimental validation of the proposed scheme applied for EV propulsion structure via a test bench, which constitute others interesting topics, will be the subject of future works.

NOMENCLATURE

v_s	Stator voltage αβ-vector
i_s	Stator current αβ-vector
ϕ_s	Stator flux αβ-vector
R_s, R_r	Stator and rotor resistances
L_s, L_r	Global stator, and rotor self-inductances of each armature
M	Global mutual inductance between stator and rotor armatures
m	Mutual inductance between two phases, stator, and rotor, where $m = \frac{2}{3}M$
ω_s	Synchronous angular speed
j	Imaginary unit, satisfying $j^2 = -1$
θ	Flux stator angle
p	Number of pole pairs
T_e	Electromagnetic torque
(.)*	Input command variable
i_{sc}	Current flowing through the short circuit winding
Ω	Mechanical speed
Ω_1, Ω_2	Speeds of left motor and right motor
Ω_o^*, Ω_{diff}^*	EV speed command, the speed difference
J	Rotor Inertia
PI	Proportional Integral controller

APPENDIX

Table 1

Induction motor parameters

Parameters	Values
Power	4 kW
Voltage	220/380 V
Frequency	50 Hz
+ Eventual three-phase boost transformer with ratio 1/20 adapted to voltage battery	
R_s	1.2 Ω
R_r	1.8 Ω
L_s=L_r	0.1564 H
M	0.15 H
J	0.07 Kg.m^2
p	2

Received on 14 September 2021

REFERENCES

1. Toufik Roubache, Souad Chaouch, Mohamed-Saïd Naït-Saïd, *Backstepping design for fault detection and FTC of an induction motor drives-based EVs*, Automatika, **57**, *3*, pp 736–748 (2016).
2. P. Gangsar, R. Tiwari, *Signal based condition monitoring techniques for fault detection and diagnosis of induction motors: A state-of-the-art review*, Mechanical Systems and Signal Processing, **144**, pp. 1–37 (2020).
3. S Bindu, Vinod V Thomas, *Diagnoses of internal faults of three-phase squirrel cage induction motor – A review*, International Conference on Advances in Energy Conversion Technologies IEEE (ICAECT), Manipal, India, 2014, pp. 48–54.
4. S. Nandi, H.A. Toliyat, X. Li, *Condition monitoring and fault diagnosis of electrical motors – A review*, IEEE Trans. Energy Conversion, **20**, *4*, pp. 719–729 (2005).

5. M. Riera-Guasp, J.A. Antonino-Daviu, G.-A. Capolino, *Advances in electrical machine, power electronic, and drive condition monitoring and fault detection: State of the art*, IEEE Trans. Ind. Electron., **62**, 3, pp. 1746–1759 (2015).
6. M.A. Mazzoletti, G.R. Bossio, C.H. De Angelo, D.R. Espinoza-Trejo, *A model-based strategy for inter turn short-circuit fault diagnosis in PMSM*, IEEE Transactions on Industrial Electronics, **64**, *9*, pp. 7218–7228 (2017).
7. Y. Wu, B. Jiang, Yulong Wang, *Incipient winding fault detection and diagnosis for squirrel-cage induction motors equipped on CRH trains*, ISA Transactions, **99**, pp. 488–495 (2020).
8. J.B. Teguia, G.C. Fouokeng, G.P. Kenne, *Induction motor windings faults detection using active and reactive power based model reference adaptive system estimator*, Int. J. of Progressive Sciences and Technologies (IJPSAT), **23**, *2*, pp. 66–86 (2020).
9. S.S. Dhamal, M.V. Bhatkar, *Modelling and simulation of three-phase induction motor to diagnose the performance on inter-turn short circuit fault in stator winding*, International Conference on Computing, Power and Communication Technologies (GUCON), Greater Noida, UP, India, Sept. 28–29, 2018, pp. 1166–1172.
10. A.V.J.S. Praneeth, S.S. Williamson, *Algorithm for prediction and control of induction motor stator interturn faults in electric vehicles*, IEEE Transportation Electrification Conference and Expo (ITEC), Chicago, USA, June 22–24, 2017, pp. 130–134.
11. A. Gandhi, T. Corrigan, L. Parsa, *Recent advances in modeling and online detection of stator interturn faults in electrical motors*, IEEE Trans. on Ind. Electronics, **58**, *5*, pp. 1564–1575 (2011).
12. K.N. Gyftakis, A.J.M. Cardoso, *Reliable detection of stator interturn faults of very low severity level in induction motors*, IEEE Transactions on Industrial Electronics, **68**, *4*, pp. 3475–3484 (2020).
13. S. M.A. Cruz, A.J.M. Cardoso, *Stator winding fault diagnosis in three-phase synchronous and asynchronous motors, by the extended Park's vector approach*, IEEE Transactions on Industry Applications, **37**, *5*, pp. 1227–1233 (2001).
14. L. Heming, S. Liling, X. Boqiang, *Research on transient behaviors and detection methods of stator winding inter-turn short circuit fault in induction motors based on multi-loop mathematical model*, IEEE International Conference on Electrical Machines and Systems, Nanjing, China, 27–29 Sept. 2005, pp. 1951–1955.
15. G.H. Bazan, P.R. Scalassara, W. Emdo, A. Goedtel, R.H.C. Palacios, W.F. Godoy, *Stator short-circuit diagnosis in induction motors using mutual information and intelligent systems*, IEEE Trans. on Ind. Electronics, **66**, *4*, pp. 3237–3246 (Apr. 2019).
16. S. Bachir S. Tnani, J.C. Rigeassou, G. Champenois, *Diagnosis by parameter estimation of stator and rotor faults occurring in induction machines*, IEEE Transactions on Industrial Electronics, **53**, *3*, pp.963–973 (2006).
17. M. Bouzid, G. Champenois, *A novel reliable indicator of stator windings fault in induction motor extracted from the symmetrical components*, IEEE Int. Symposium on Ind. Electronics Conference, Gdansk, Poland, 27–30 June 2011, pp. 489–495.
18. A. El Kharki, Z. Boulghasoul, L. Et-Taaj, Z. Kandoussi, A. Elbacha, *Real-time implementation of backstepping control for high performances induction motor drive*, 4th World Conference on Complex Systems (WCCS), Ouarzazate, Morocco, 22-25 April, 2019.
19. R. Trabelsia, A. Khedher, M.F. Mimouni, F. M'sahli, *Backstepping control for an induction motor using an adaptive sliding rotor-flux observer*, Electric Power Systems Research, **93**, pp. 1–15 (December 2012).
20. S. Vaidyanathan, A.T. Azar, *Backstepping control of nonlinear dynamical systems*, 1st edition, Academic Press, 2020, pp. 1–515.
21. M. Horch, A. Boumediene, L. Baghli, *Backstepping approach for nonlinear super twisting sliding mode control of an induction motor*, 3rd International Conference on Control, Engineering & Information Technology (IEEE CEIT 2015), Tlemcen, Algeria, 25-26 May, 2015.
22. T. Ameid, A. Menacer, R. Romary, R. Pusca, H. Talhaoui, *DWT for rotor bars fault detection applied to Backstepping control induction motor drive in low-speed*, 43th Annual Conf. of the IEEE Ind. Electronics Society, 29 Oct.–1 Nov., 2017, pp. 8059–8064.
23. S.S. Dhamal, M.V. Bhatkar, *Modelling and simulation of three-phase induction motor to diagnose the performance on inter-turn short circuit fault in stator winding*, International Conference on Computing, Power and Communication Technologies (GUCON), Greater Noida, India, 28-29 Sept., 2018, pp. 1166–1172.
24. A. Hamoudi, B. Kouadri, *On-line stator winding inter-turn short-circuits detection in induction motors using recursive levenberg-marquardt algorithm*, International Journal on Electrical Engineering and Informatics, **9**, *1*, pp. 42–57 (2017).
25. M. Bouakoura, M.-S. Nait-Said, N. Naït-Saïd, *Incipient inter-turn short circuit fault estimation based on a faulty model observer and ann-method for induction motor drives*, Recent Advances in Electrical & Electronic Engineering, **12**, pp. 1–7 (2019).
26. D. Benoudjit, N. Nait-Said, M-S, Nait-Said, *Differential speed control of a propulsion system using fractional-order controller*, Electromotion J., **14**, *2*, pp. 91–98 (2007).